Gravitational microlensing of gamma-ray burst afterglows by single and binary stars

Share Your Story

Gravitational Microlensing of Gamma-Ray Burst Afterglows by Single and Binary Stars

Shude Mao[1] and Abraham Loeb[2]

[1] Univ. of Manchester, Jodrell Bank Observatory, Macclesfield, Cheshire SK11 9DL, UK

[2] Harvard-Smithsonian CfA, 60 Garden Street, Cambridge, MA 02138, USA

ABSTRACT

We calculate the magnification light curves due to stellar microlensing of gamma-ray burst (GRB) afterglows. A GRB source appears on the sky as a thin ring which expands faster than the speed of light and is maximally magnified as it crosses the lens caustics. While a single star lens produces a single peak in the magnification light curve, binary star lenses may produce multiple peaks. The shape of the magnification light curve provides invaluable information on the surface brightness distribution of the afterglow photosphere on sub micro-arcsecond scales. We find that *all* afterglows are likely to show variability at the level of a few percent about a year following the explosion, due to stars which are separated by tens of Einstein radii from their line-of-sight.

Subject headings: cosmology: theory – gamma rays: bursts – gravitational lensing – stars: binaries

1.   Introduction

The lensing cross-section of a star at cosmological distances is defined by the Einstein angle,

$$\theta_{\rm E} = \left(\frac{4GM_{\rm lens}}{c^2 D}\right)^{1/2} = 1.6 \left(\frac{M_{\rm lens}}{1 M_\odot}\right)^{1/2} \left(\frac{D}{10^{28}\ {\rm cm}}\right)^{-1/2}\ {\rm micro-arcsecond}, \qquad (1)$$

where $M_{\rm lens}$ is the lens mass, $D \equiv D_{\rm os} D_{\rm ol}/D_{\rm ls}$ is the ratio of the angular-diameter distances between the observer and the source, the observer and the lens, and the lens and the source (Schneider, Ehlers, & Falco 1992, p. 27). Typical astrophysical sources and lenses move at speeds of $v \lesssim 10^3$ km s^{-1}, and hence produce a characteristic event duration of $\sim D_{\rm os}\theta_{\rm E}/v \gtrsim$ 25 years for solar mass lenses.

Coincidentally, the apparent angular size of gamma-ray burst (GRB) afterglows is also of order a micro-arcsecond, i.e. comparable to the Einstein angle of a solar mass lens at a cosmological distance. Loeb & Perna (1998) noted that the highly relativistic expansion of these sources would shorten considerably the duration of their microlensing events. A GRB afterglow is predicted to appear on the sky as a narrow ring which expands laterally at a superluminal speed, $\sim \Gamma c$, where $\Gamma \gg 1$ is the Lorentz factor of the relativistic blast wave which emits the afterglow radiation (Waxman 1997b; Sari 1998; Panaitescu & Meszaros 1998; Granot, Piran, & Sari 1999). For $\Gamma \sim 10$ the event duration is shortened by 3–4 orders of magnitude relative to typical astrophysical sources, and is reduced to the convenient timescale of days. Recently, Garnavich, Loeb, & Stanek (2000) have reported the possible detection of a microlensing magnification feature in the optical-infrared light curve of GRB 000301C. The achromatic bump in the light curve is well fitted by a microlensing event of a $0.5 M_\odot$ lens separated by an Einstein angle from the source center, as long as the source is a ring with a narrow fractional width ($\sim 10\%$), in accordance with earlier theoretical predictions. In a case similar to GRB sources, Koopmans & de Bruyn (2000) have recently reported evidence for intra-day radio microlensing in the lens B1600+434 due to superluminal motions of the lensed source. On a longer-time scale, microlensing of the lensed QSO 2237+0305 had been observed over many years and more recently in real-time (Wozniak et al. 2000 and references therein).

The predicted angular size of GRB afterglows was already confirmed through the detected transition from diffractive to refractive scintillations in the radio afterglow of GRB 970508 (Goodman 1997; Waxman, Kulkarni, & Frail 1998). Unfortunately, scintillations are not a sufficiently delicate probe to provide information about the ring-like surface brightness distribution of a GRB source on the sky. On the other hand, microlensing can resolve the sub micro-arcsecond structure of GRB photospheres as a function of observed photon frequency. In this *Letter*, we expand the original discussion of Loeb & Perna (1998) on single star lenses, and calculate the magnification light curve for two other lens configurations, namely binary star lenses and a single star in an external shear field (due to the gravitational potential of the host galaxy or a distant binary companion). These lensing configurations are more likely to describe stars which are embedded in the luminous cores of galaxies. At cosmological distances, the simple model of single star lensing is adequate only for stars which reside in the outer regions of galaxies or in the intergalactic medium.

The probability for having an intervening lens star within a projected angular separation θ from a source at a redshift $z \sim 2$ is $\sim 0.3\Omega_\star(\theta/\theta_{\rm E})^2$ (Press & Gunn 1973; Blaes & Webster 1992; Nemiroff 1998; Nemiroff et al. 1998), where $\Omega_\star$ is the cosmological density parameter of stars. The value of $\Omega_\star$ is bounded between the density of the luminous stars in galaxies and the total baryonic density as inferred from big bang nucleosynthesis, $7 \times 10^{-3} \lesssim \Omega_\star \lesssim 5 \times 10^{-2}$

(Fukugita, Hogan, & Peebles 1998). Hence, all GRB afterglows should show evidence for events with $\theta \lesssim 20\theta_{\rm E}$, for which microlensing provides a small perturbation to the light curve[1]. In this *Letter*, we calculate the magnification light curves of such events, as well as light curves of rarer events with a smaller impact parameter – for which the peak amplitude is larger.

In §2 we describe the method of our calculation, and in §3 we present our numerical results. Finally, §4 summarizes the main implications of these results.

2. Method of Calculation

We assume that the GRB source appears on the sky as an inner disk with a uniform surface brightness bounded by a uniform outer ring. This model has the minimum number of free parameters, which are necessary to describe results from detailed calculations (see Figs. 11 and 12 in Granot et al. 1999). We specify the ratio between the surface brightness of the inner disk and that of the outer ring using a contrast parameter, C. In reality, the contrast C and the ring fractional width W, depend on photon frequency and obtain different values for the different spectral slope regimes that are separated by spectral breaks in an afterglow spectrum (Sari, Piran, & Narayan 1998; Granot et al. 1999). The outer boundary of the ring is determined by the sharp cut-off in relativistic beaming at angles $\gtrsim 1/\Gamma$ relative to the center of the explosion. The dimming of the inner disk of the image results from the fact that the outer ring suffered a longer geometric time delay and hence must have been emitted at earlier times – when the fireball was brighter.

The ring-like image of the source expands outwards at a superluminal speed, and so the lens is assumed to be stationary. During the relativistic expansion of a spherical fireball, the apparent source radius increases with time as $\propto t^{5/8}$ (Waxman 1997b; Loeb & Perna 1998). The effects of lensing on the source image depend only on its angular structure in units of the Einstein angle, $\theta_{\rm E}$; this angle, given in equation (1), is a function of the source and lens redshifts and the lens mass. Hence, we normalize all angular scales in units of $\theta_{\rm E}$ and parametrize the time-dependent angular radius of the ring as,

$$R_{\rm s}(t) = R_0 t^{5/8}, \tag{2}$$

where R_0 is the angular radius of the outer ring in units of the $\theta_{\rm E}$ after one day, and t is the time in days. For binary lenses, we take $M_{\rm lens}$ to be the total mass of the system. For

---

[1]This crude estimate ignores the need to subtract those stars which are embedded in the dense central regions of galaxies, where macrolensing dominates and the microlensing optical depth is of the order of unity.

definitiveness, we adopt a value of $R_0 = 0.5$, as found by Garnavich, Loeb & Stanek (2000) for GRB 000301C. The time axis in our plots can be trivially rescaled by $R_0^{-8/5}$ for other choices of R_0.

We note that equation (2) is adequate only as long as the GRB fireball is spherically-symmetric and highly relativistic. A collimation of the outflow into a jet changes this scaling as soon as the fireball Lorentz factor decelerates to a value smaller than the inverse of the collimation angle (Rhoads 1997). Eventually, the total energy release is isotropized (as if it came from a quasi-spherical explosion) after the fireball enters the non-relativistic stage of its expansion. Using the geometric time-delay of the ring and the Blandford-McKee (1976) self-similar solution for the expansion of a relativistic spherical fireball, one finds that the Lorentz factor of the blast wave at an observed time t is given by, $\Gamma \approx 6.4(E_{52}/n_0)^{1/8}t^{-3/8}$, where E_{52} is the (isotropically-equivalent) energy release in units of 10^{52} erg s^{-1} and n_0 is the number density of the ambient gas in units of 1 cm^{-3} (e.g., Waxman 1997a,b). Hence, the shock wave is expected to become non-relativistic several months after the explosion. In the non-relativistic regime, the source follows the Sedov-Taylor self-similar scaling of $R_s \propto t^{2/5}$, and the ring contrast is determined solely by the limb-brightening effect. Since no calculations were done so far to describe the evolution of the source image on the sky for collimated outflows or during the transition to the non-relativistic regime, and since the power-law index of $2/5 = 0.4$ is not very different from $5/8 = 0.625$, we assume for simplicity that the fireball is spherically-symmetric and adopt equation (2) as a crude approximation for the expansion of the source on the sky up to a year after the GRB trigger. The detailed evolution of the source image requires elaborate numerical calculations, and its magnification by a simple point mass lens will be considered elsewhere (Granot & Loeb 2000). Here we adopt a simple source model and focus on the properties of more complex lens systems.

We consider three types of lenses: a single point-mass, a single point-mass with external gravitational shear, and a binary star lens. The effect of the host galaxy on the microlens is well described by the second case. The third case corresponds to a situation when two stars are sufficiently close together so that they act coherently as a binary lens. About forty binary lensing events have been detected so far in microlensing searches in the local group (Alcock et al. 2000a; Udalski et al. 2000).

For the single star lens, we choose the origin to be at the lens position and define the source properties by R_0, W, and C. The angular separation between the lens and the source center is parametrized by $b \equiv \theta/\theta_E$. For the star+shear case, the lens is located again at the origin, and the shear is oriented along the x-axis, with its strength given by γ (e.g., Mao 1991). For a primary lens M_{lens}, a perturbative lens of mass m at distance r will provide a shear $\gamma = m/r^2$, where m is in units of M_{lens} and r is in units of the Einstein radius

corresponding to mass M_{lens}. For the binary case, the two lenses are parametrized by a mass ratio, q, and separation, a, with the origin centered at the mid-point of the lenses. In both cases, the source center is specified by some point $(x_{\mathrm{c}}, y_{\mathrm{c}})$.

In all three cases, the lens equation can be manipulated into a complex polynomial using a complex coordinate notation (Witt 1990; Mao 1991; Witt & Mao 1994). The associated polynomial can be readily solved using well-known numerical schemes (e.g., Press et al. 1992) to yield the image positions and magnifications for any source position. Given our assumed source profile, the magnification is given by (see Eq. 8 in Loeb & Perna 1998)

$$\mu(R_{\mathrm{s}}, W, C) = \frac{\Psi(R_{\mathrm{s}}) - (1 - C)(1 - W)^2 \Psi[(1 - W)R_{\mathrm{s}}]}{1 - (1 - C)(1 - W)^2,} \tag{3}$$

where $\Psi(R_{\mathrm{s}})$ is the magnification for a uniform surface-brightness disk of radius R_{s}. While the calculation of $\Psi(R_{\mathrm{s}})$ is straightforward for the single star case (e.g., Witt & Mao 1994; Schneider et al. 1992, p. 313), it is no longer simple for the star+shear case and for the binary lens case. For these two cases, one has to integrate over the singularities in the magnification amplitude as the expanding source sweeps across the lens caustics. Equation (3) only requires knowledge of the magnification for a uniform source of radius R (where $R = R_{\mathrm{s}}$ or $(1-W)R_{\mathrm{s}}$). Since gravitational lensing conserves surface brightness, the magnification of each image is simply the ratio of the image area to the source area, πR^2.

In order to find the image area using Stokes theorem, we only need to solve the lens equation for the mapping of the confining circle (Gould & Gaucherel 1997; Dominik 1998). We therefore place n points on the circle and distribute them uniformly in angle. For each point we then solve the lens equation to obtain the corresponding image positions. We then connect the image positions into continuous image tracks. In general, there are several non-crossing, closed, image tracks. The two insets in Fig. 3 show two examples of image tracks for a binary lens configuration (see §3 for lens parameters). In each inset, the thin solid line with cusps is the caustic. A point source located on the caustic would be infinitely magnified with its images projected on the critical curve, shown as the dashed line. The left inset presents the image tracks for a source center which is located inside the caustic. In this case, the confining circle of the source (dotted line) is mapped into five disjoint image tracks (with the central track being highly demagnified and hence too small to be seen). The right inset shows a source that intercepts the caustics. In this case, the confining circle is mapped into two tracks, one of which is embedded within the other. If the image tracks are not embedded within each other (such as the case shown in the left inset) then the total magnification is simply the ratio between the total area they confine and πR^2. However, for image tracks that are embedded inside each other, special care needs to be applied. If an image track is confined within other image tracks for an odd (even) number of times, then

one needs to subtract (add) the area confined by the track. For example, in the right inset the total area is found by subtracting the area enclosed by the inner track from the area enclosed by the outer track. To achieve convergence, we double the number of points on the circle to $2n$ until the magnification value is within 0.01% of that found in the previous iteration. In this *Letter*, we only show the magnification history. The observed light curves can be easily obtained by multiplying the unlensed (power-law) afterglow light curve with the magnification amplitude at each time.

3. Results

The microlensing probability scales as the square of the impact parameter from the line-of-sight to the source. For $\Omega_\star \sim 0.01$, most GRB afterglows would be separated by several tens of $\theta_{\rm E}$ from a star. Figure 1 shows the magnification light curves of a single star for $b = 10$ and $b = 20$. In such cases, the magnification light curve generically gives a peak amplitude of a few percent about a year after the GRB trigger. By considering a large statistical sample of GRBs, one may be able to identify a systematic feature of this type and constrain $\Omega_\star$. However, it is important to remember that the predicted microlensing signature may change considerably at late times for collimated outflows.

The magnification light curves depend on the surface brightness distribution of the source image. Figure 2 shows the light curves for different choices of W and C with an impact parameter $b = 1$. The three solid curves show the magnification for $C = 0$ and the three cases of $W = 0.05, 0.1$ and 0.2. As the ring width increases, the peak magnification drops but the full width at half maximum increases. The dotted and dashed lines show two other examples for $C = 0.5$ and 1, respectively. In both cases, $W = 0.05$. Compared with the case of the same W but with $C = 0$ (solid line with the highest peak magnification), it is evident that the increase in C from 0 to 0.5 broadens the magnification curve considerably, although the additional increase from 0.5 to 1 results in a much milder effect.

Figure 3 shows two examples of the more complex light curves that result from binary star lenses. The two lenses have equal-mass and a separation $a = 0.8$, and we adopt $W = 0.1$ and $C = 0$ for the source. The insets in Figure 3 illustrate the lens positions, and the resulting caustics and critical curves. For the left inset, the source center is at the origin, while for the right inset the source center is at $(-0.16, -1)$. For each inset, the image tracks for the dotted circle are indicated by thick solid lines (see §2). The light curves show multiple peaks due to different caustic crossings. Just as found in Galactic binary microlensing events (Alcock et al. 2000a; Udalski et al. 2000, and references therein), the set of possible light curves is diverse. However, the magnification light curves of GRB afterglows obtain smaller peak amplitudes

and do not exhibit features as sharp as their Galactic counterparts. These differences result from the different source profiles; while Galactic stars have radii ($\sim R_\odot$) which are three orders of magnitude below the Einstein radius of their lenses, GRB afterglows obtain a size which is comparable to the Einstein radius and hence smooth the magnification pattern over their extended image.

Finally, Figure 4 shows the effect of an external shear on the magnification light curve with $W = 0.1$ and $C = 0$. The solid lines show three cases where the source center is at $(x_c, y_c) = (1, 0)$, with the shear amplitude increasing in strength from 0 to 0.2. For $\gamma \lesssim 0.1$, the shear changes the initial magnification mildly, while for $\gamma = 0.2$, the magnification actually drops during the initial expansion phase. Since the shear breaks the spherical symmetry of a single lens, we show by the dotted and dashed lines the magnification light curves for $\gamma = 0.1$ and 0.2 respectively, but with the source center located on the y axis at $(x_c, y_c) = (0, 1)$. Compared with the case with no shear, the light curve changes are relatively minor; they show a slight decrease in the initial magnification followed by an offset in the time of peak magnification. For a single star residing in an isothermal galactic potential of a 1D velocity dispersion σ, the external shear is $\gamma = \theta_{cr}/(2\theta)$, where θ is the angle between the line of sight and the galaxy center, and $\theta_{cr} = 4\pi(\sigma/c)^2 D_{ls}/D_{os}$ is the critical angle for multiple imaging, which is typically $\lesssim 1$ arcsecond (see Schneider et al. 1992, §8.1.4). Hence, unless the line-of-sight of the GRB passes through the central region of an intervening galaxy, the shear is likely to be much smaller than unity and hence its effect on the magnification light curve would be modest.

4. Discussion

We have found that all GRB afterglows are likely to show a microlensing amplification bump of a few percent after about a year (Fig. 1). The peak magnification and its timing depend strongly on the impact parameter. A smaller impact parameter results in an earlier and a higher peak magnification. For $b \gtrsim 2$, the peak magnification is usually reached when the limb of the source crosses the lens. Equation (2) implies that the time of peak magnification is then $t_{peak} \approx (b/R_0)^{8/5}$. Numerically, we find that the peak magnification scales roughly as $\mu_{peak} \approx 1 + 2.5(W/0.05)^{-1/2} b^{-3/2}$ for $C = 0$. The *Swift* satellite [2], planned for launch in 2003, will provide trigger and good localization for hundreds of GRB afterglows per year. Identification of the statistics of such features can be used to constrain $\Omega_\star$. A remaining important question is how the optical depth for microlensing (or the associated

---

[2] see http://swift.sonoma.edu/

shear) is distributed along the line of sight. While stars in the halos of galaxies are likely to be in the regime of very small optical depth, the outer disk or spheroid stars will be surrounded by a modest optical depth with a significant shear, while stars in the cores of galaxies are in the high optical depth regime where the GRBs are likely to be multiply imaged. The relative abundance of stars in these populations can be, in principle, calibrated based on ongoing microlensing studies of the Milky Way galaxy (Alcock et al. 2000b, and references therein).

The detailed shape of the magnification light curve depends on the contrast, C, and fractional width, W, of the ring-like afterglow image (Fig. 2). The values of these parameters should change in a predictable way across spectral breaks (e.g. when comparing radio to optical-infrared data), because of the corresponding change in the structure of the source image on the sky (Granot et al. 2000). Detailed multi-frequency monitoring of a microlensing event, similar or better than the data used by Garnavich et al. (2000), could provide invaluable information on the sub micro-arcsecond structure of GRB photospheres.

We have also found that binary lenses produce multiple peaks in the magnification light curves (Fig. 3). However, an external shear has only a modest effect on the magnification history, changing its early time amplitude from the constant value which characterizes the zero shear case, but not affecting much its late evolution. While the zero shear lens does not resolve the source when the angular size of the source is much smaller than its impact parameter relative to the lens, the star+shear lens provides information about the expansion of the source even at these early times. The light curves of both the star+shear lens and the binary lens are determined by a small number of parameters. For example, the binary light curves are fixed by two binary parameters (separation and mass ratio) and five parameters that describe the source properties: the source center position (x_c, y_c), R_0, W and C [see Eqs. (2) and (3)]. Similarly to the known binary microlensing events toward the Galactic and Magellanic Clouds, it should be possible to infer the lens and source parameters such as W, C and R_0 from a densely-sampled light curve. The values of these parameters at various photon frequencies would in turn provide new constraints on the energy output and ambient gas density of GRB fireballs, and hence on the central engines that power them.

REFERENCES

Alcock, C. et al. 2000a, ApJ, 541, 270

——————. 2000b, ApJ, 542, 281

Blaes, O. M., & Webster, R. L. 1992, 391, L63

Blandford, R. D., & McKee, C. F. 1976, Phys. Fluids, 19, 1130

Dominik, M. 1998, A&A, 333, L79

Fukugita, M., Hogan, C. J., & Peebles, P. J. E. 1998, ApJ, 503, 518

Garnavich, P. M., Loeb, A., Stanek, K. Z. 2000, ApJ, in press (astro-ph/0008049)

Goodman, J. 1997, New Astronomy, 2, 449

Granot, J., & Loeb, A. 2000, in preparation

Gould, A. Gaucherel, C. 1997, ApJ, 477, 580

Granot, J., Piran, T., & Sari, R. 1999, ApJ, 513, 679

Koopmans, L. V. E., de Bruyn, A. G. 2000, A&A, 358, 793

Loeb, A., & Perna, R. 1998, ApJ, 495, 597

Mao, S. 1991, ApJ, 389, 63

Nemiroff, R. 1998, Ap& SS, 259, 309

Nemiroff, R., Norris, J. P., Bonnell, J. T., & Marani, G. F. 1998, ApJ, 494, L173

Panaitescu, A., & Meszaros, P. 1998, 493, L31

Press, W. H., & Gunn, J. E. 1973, ApJ, 185, 397

Press, W. H., Teukolsky, S. A., Vetterling, W. T., & Flannery, B. P. 1992, Numerical Recipes
    in Fortran (NY: CUP), p. 367

Rhoads, J. E. 1997, ApJ, 487, L1

Sari, R. 1998, ApJ, 494, L49

Sari, R., Piran, T., & Narayan, R. 1998, ApJ, 497, L17

Schneider, P., Ehlers, J., & Falco, E. E. 1992, Gravitational Lenses (Heidelberg: Springer)

Udalski, A., Zebrun, K., Szymanski, M., Kubiak, M., Pietrzynski, G., Soszynski, I., Wozniak,
    P. 2000, AcA, 50, 1

Waxman, E. 1997a, ApJ, 489, L33

——————. 1997b, ApJ, 491, L19

Waxman, E., Kulkarni, S., & Frail, D. A. 1998, ApJ, 497, 288

Witt, H. J. 1990, A&A, 236, 311

Witt, H. J., & Mao, S. 1994, ApJ, 430, 505

Wozniak, P. R., Udalski, A., Szymanski, M., Kubiak, M., Pietrzynski, G., Soszynski, I., &
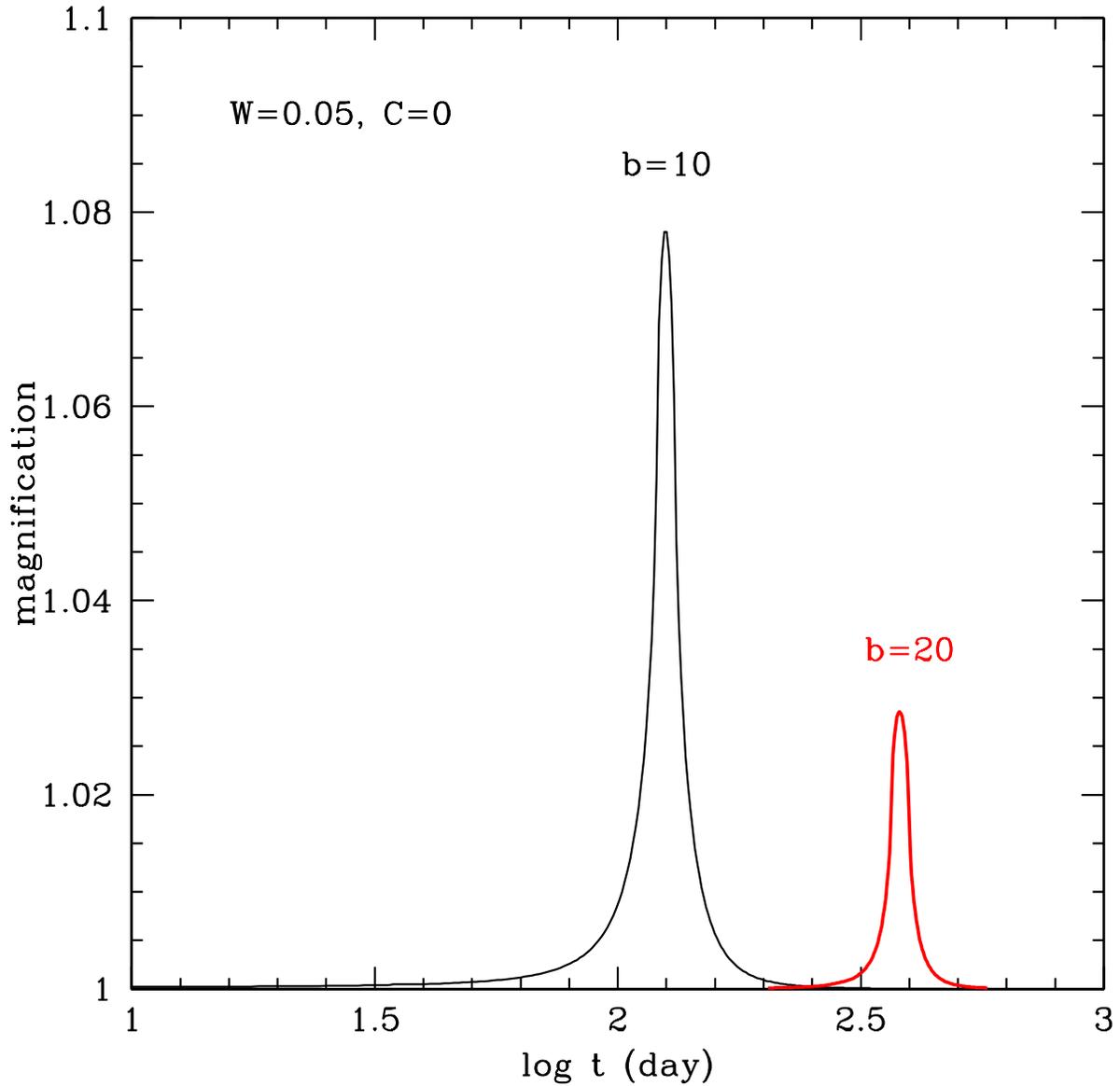Zebrun, K. 2000, ApJ, 540, L65

Fig. 1.— The afterglow magnification as a function of time for a single star lens. The two curves correspond to an impact parameter of the source center relative to the lens of $b = 10$ and 20, in Einstein angle units. Such impact parameters should be typical for any GRB, given the density of stars in the Universe. The GRB source is assumed here to be a narrow ring with a fractional width $W = 0.05$.
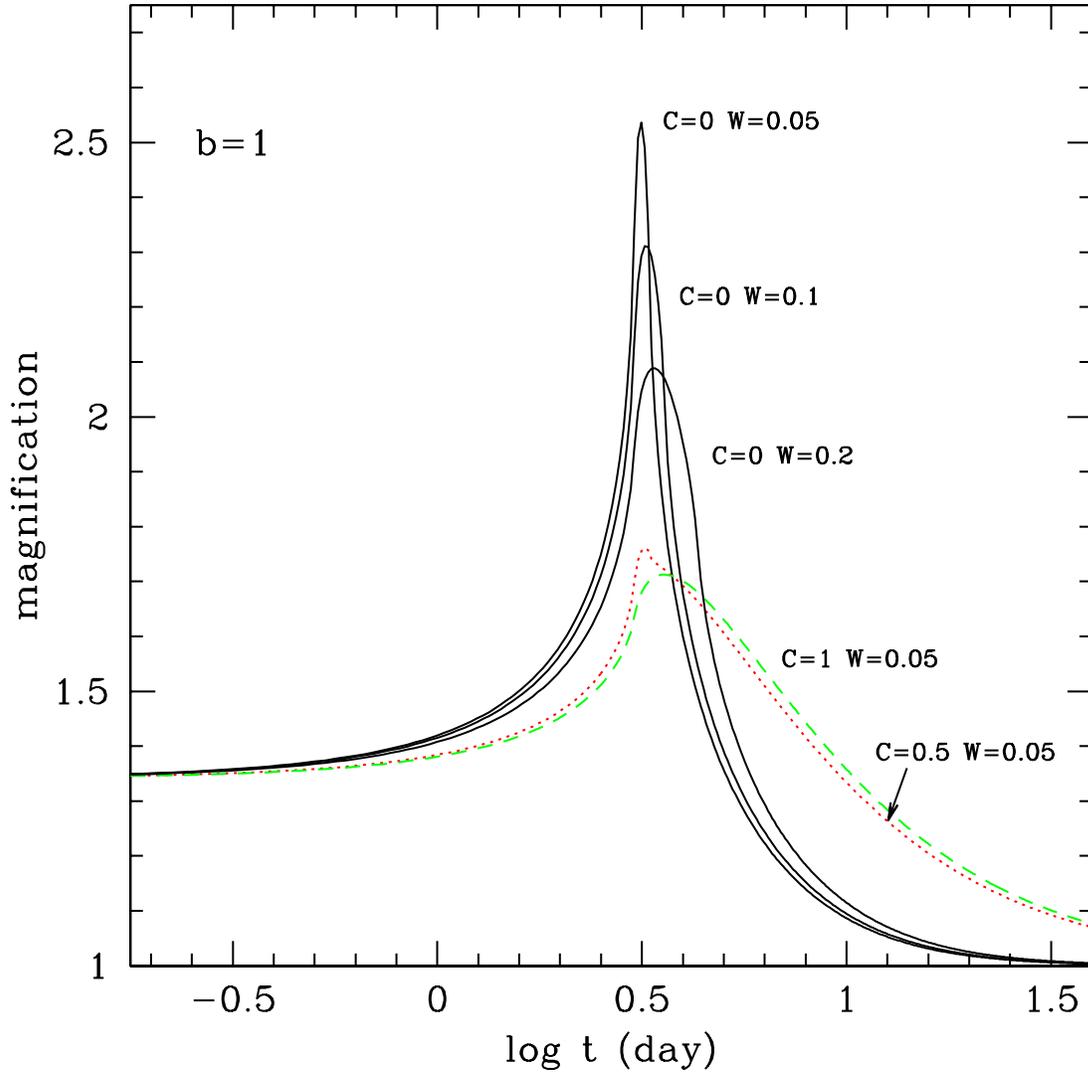
Fig. 2.— The magnification history for different source profiles and a single star lens at an impact parameter $b = 1$.
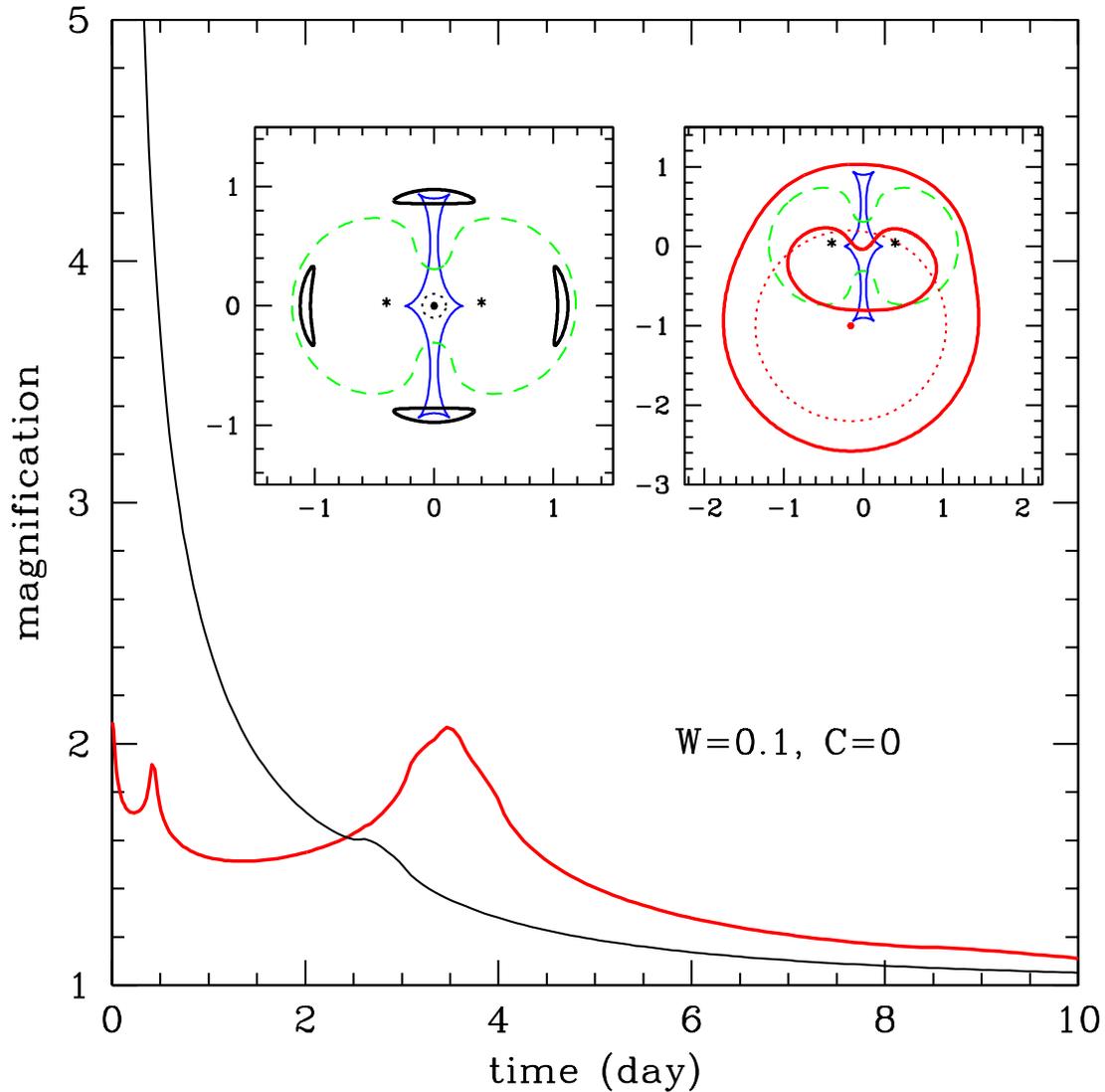
Fig. 3.— The magnification history for a binary lens with equal mass stars at a separation of $a = 0.8$ in Einstein angle units. The two insets show different cases for the location of the source center (filled dots). In the left inset, the source center is inside the caustic region, while in the right inset the source is close to but outside the caustic. The positions of the two lens stars are labelled by star symbols. The thin solid line with cusps is the caustic while the dashed line is the critical curve. The image tracks for the dotted circle are shown as thick solid lines in the insets. The thin and thick lines in the magnification light curves correspond to the left and right insets, respectively. Note that the location of the origin and the axis scales are different in the two insets.
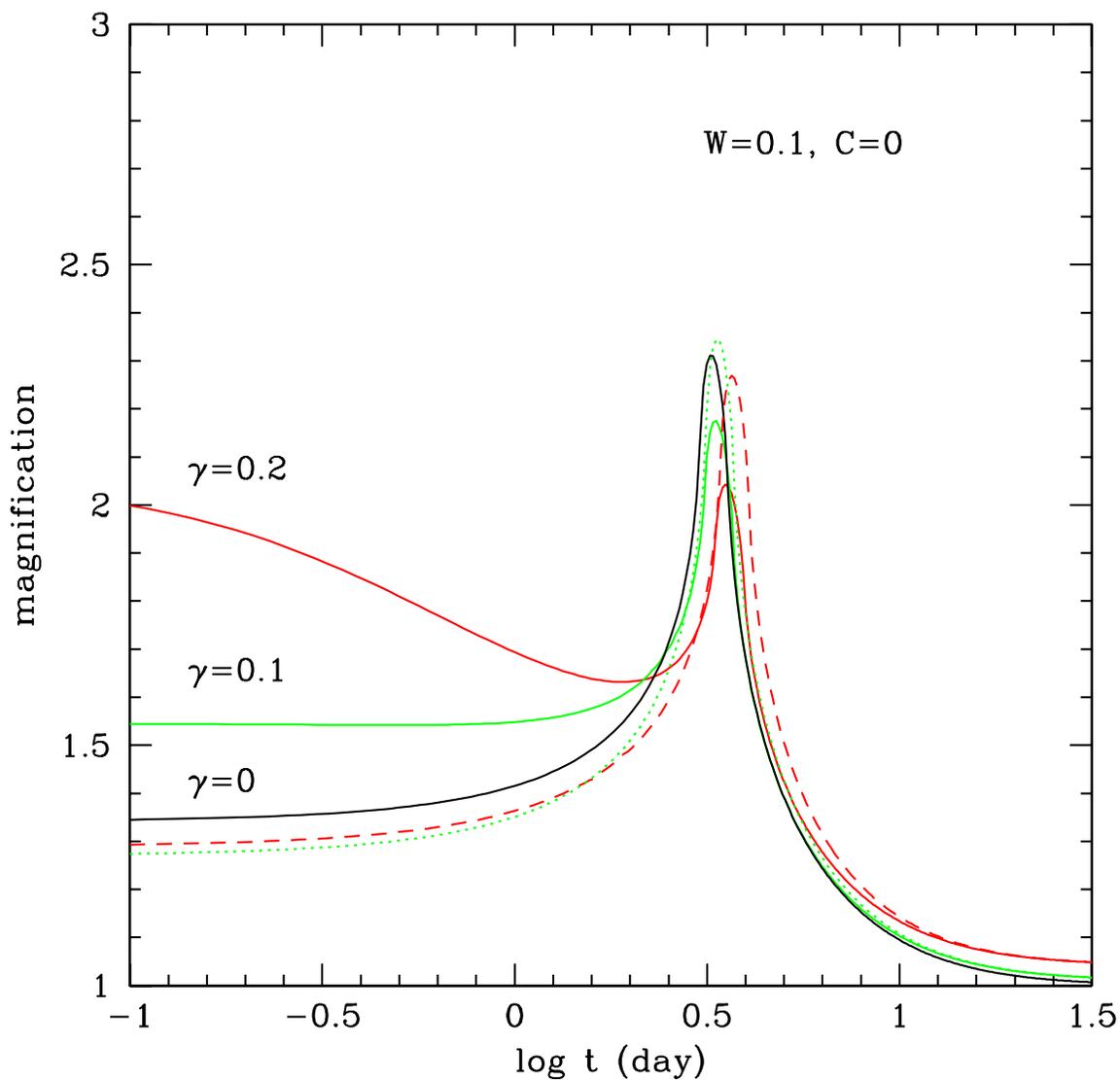
Fig. 4.— The magnification history for a single star embedded in an external shear, γ. The three solid lines are for $\gamma = 0, 0.1, 0.2$, respectively and with the source center on the x-axis, $(x_c, y_c) = (1, 0)$. The dotted and dashed lines have $\gamma = 0.1$ and 0.2, respectively, with the source center on the y-axis, $(x_c, y_c) = (0, 1)$. In all cases, we take $W = 0.1, C = 0$.